Title

The effect of calcium-magnesium mixtures in sol-gel coatings on bone tissue regeneration

Authors

Andreia Cerqueira[1*], Iñaki García-Arnáez[2*], María Muriach[3], Mikel Azkargorta[4], Félix Elortza[4], Raúl Izquierdo[1], Francisco Romero-Gavilán[1&], Mariló Gurruchaga[2], Julio Suay[1], Isabel Goñi[2]

[1]Department of Industrial Systems Engineering and Design, Universitat Jaume I, Av. Vicent Sos Baynat s/n, 12071 Castellón de la Plana, Spain

[2]Departament of Science and Technology of Polymers, Universidad del País Vasco, P. M. de Lardizábal, 3, 20018 San Sebastián, Spain

[3]Deparment of Medicine, Universitat Jaume I, Av. Vicent Sos Baynat s/n, 12071 Castellón de la Plana, Spain

[4]Proteomics Platform, CIC bioGUNE, Basque Research and Technology Alliance (BRTA), CIBERehd, ProteoRed-ISCIII, Bizkaia Science and Technology Park, 48160 Derio, Spain

*Co-authors

[&]Corresponding autor: Francisco Romero-Gavilán

Departamento de Ingeniería de Sistemas Industriales y Diseño

Avda. Vicent Sos Baynat s/n, Campus del Ríu Sec

12071 – Castelló de la Plana (España)

E-mail: gavilan@uji.es

Abstract

Calcium and magnesium are two elements essential for bone structure and metabolism. However, their synergistic or competitive effects on bone regeneration are often overlooked during biomaterial development. We examined the interactions between Ca and Mg in sol-gel coatings doped with mixtures of $CaCl_2$ (0.5%) and $MgCl_2$ (0.5, 1, and 1.5%). After physicochemical characterisation, the materials were incubated *in vitro* with MC3T3-E1 osteoblastic cells and RAW264.7 macrophages, and the protein adsorption was analysed using nLC-MS/MS. The incorporation of the ions did not lead to the formation of crystalline structures and did not affect the sol-gel network cross-linking. The release of the ions did not cause cytotoxic effects at any tested concentration. The proteomic analysis showed that adding the Ca and Mg ions elevated the adsorption of proteins associated with inflammatory response regulation (*e.g.*, ALBU, CLUS, HPT, HPTR, A1AG1 and A1AG2) but decreased the adsorption of immunoglobulins. The CaMg coatings had reduced affinity to proteins associated with coagulation (*e.g.,* FA9, FA10, FA11, FA12) but increased the adsorption of proteins involved in cell adhesion (DSG1, DESP, FBLN1, ZA2G). *In vitro* assays revealed that the cellular response was affected by changing the concentration of Mg. Moreover, our results show that these differences reflect the changes in the concentrations of both ions in the mix but are not a simple additive effect.

Keywords

Biomaterials, proteomics, coagulation, inflammation, cell adhesion

1. Introduction

The application of biomaterials in bone regeneration has been extensively investigated. It is a complex task involving the interactions between the materials and cells or tissues and is affected by environmental conditions [1]. A wide variety of biological processes, such as inflammation, coagulation and osteogenesis, are associated with bone restoration [2]. Their correct functioning is essential for good implant integration.

The biomaterials for bone tissue regeneration are no longer seen as biologically passive since they can orchestrate the process of tissue regeneration. Changes in the surface texture, elasticity or chemistry can bestow useful properties such as biocompatibility, mechanical strength and controlled biodegradability [3]. Allied to the changes in surface chemistry, the delivery of bioactive agents, such as inorganic ions, can determine the outcome of implantation [4,5]. Numerous therapeutic systems delivering inorganic ions (*e.g.,* calcium, magnesium, strontium or zinc) have been developed to improve bone regeneration [6]. Many studies focus on a single element and do not take into account the synergistic or competitive effects of the cations [7], hampering the optimisation of bone regeneration processes.

Calcium ions fulfil many functions in biological systems. In the bone, calcium is one of the most important elements of the mineralised matrix; the inorganic phase of this tissue stores about 99% of Ca in the body [6]. This inorganic ion plays a prominent role in bone-growth precursor cells. It stimulates the bone synthesis pathways in osteoblasts and maintains bone homeostasis, serving as a signalling molecule between osteoblasts and osteoclasts [8]. Moreover, Ca is involved in blood coagulation, mediating platelet activation by binding to factor IXa and factor Xa, required for the tenase and prothrombin complexes [9]. Magnesium is the fourth most abundant element in the human body; the Mg^{2+} ions participate in lipid, protein, nucleic acid and ATP synthesis [4,6]. Naturally found in the bone, the Mg^{2+} is essential for the metabolism of this tissue; it stimulates bone formation and resorption [4]. The Mg ions also enhance cell adhesion [10] via affecting all the cell adhesion machinery [11] and have an anti-inflammatory potential [12,13]. Therefore, the combined effect of these two metal cations might be the modulation of protein adsorption, blood clot formation, cell adhesion and differentiation, thus ensuring the success of the bone regeneration process [14].

Studying the interfaces between the biomaterials and biological components helps us understand the mechanisms of tissue–material interactions and improve the design and development of future biomaterials [15]. The adsorption of proteins onto the material surface is one of the first events upon the implantation. Analysis of this phenomenon is a potent tool for

studying the interactions between cells or tissues and the biomaterials [15,16]. The quantities and properties of the adsorbed proteins are highly dependent on the surface properties. The process can modulate cell adhesion and the subsequent cellular events, such as proliferation and differentiation, coagulation, fibrinolysis and osteogenesis [17,18].

This study developed and characterised sol-gel coatings applied to Ti surfaces and enriched with Ca (0.5 wt%) and different amounts of Mg (0.5, 1 and 1.5 wt%). The physicochemical properties of the coatings were examined, and the protein adsorption patterns, and *in vitro* cell responses were analysed. The obtained data should improve our understanding of the effects of ion mixtures on bone regeneration processes and identify the potential synergies.

2. Materials and methods

2.1. Sol-gel synthesis and sample preparation

The sol-gel technique was used to develop hybrid coatings capable of releasing both the Ca and Mg ions. MTMOS and TEOS alkoxysilanes (molar ratio of 7:3) were mixed with 2-propanol (50% v/v). This precursor selection and its ratio were optimised in a previous study [19]. The precursors were hydrolysed by adding their stoichiometric amount of 0.1N HNO_3 at the rate of 1 drop s^{-1} under stirring. The solutions already contained the appropriate amounts of $CaCl_2$ and $MgCl_2$. The content of $CaCl_2$ was fixed at 0.5 % wt, as established in the previous study [20], whereas the $MgCl_2$ was incorporated in increasing amounts (0.5, 1, 1.5% wt) (**Table 1**). A composition without salts (MT) and another mixture only doped with Ca (without Mg; Ca) were used as controls. The different sol-gel mixtures were kept under stirring for 1 h and then left at rest for 1 h. Then, grade-4 Ti discs (1-mm thick) were sandblasted and acid-etched as described in the paper of Romero-Gavilán *et al.* [21] to be used as coating substrates. The 10-mm diameter discs were used for *in vitro* assays and the 12-mm diameter discs for proteomics and physicochemical evaluations. The synthesised sol-gel compositions were applied onto the discs using a dip-coater (KSV DC; KSV NIMA, Espoo, Finland). The immersion was performed at 60 cm min^{-1}, and after one minute, the samples were removed at 100 cm min^{-1}. For evaluation of hydrolytic degradation and the cation kinetic release, the coatings were applied onto glass slides. The glass surface was conditioned before coating in an HNO_3 solution (25% v/v) using an ultrasonic bath (Sonoplus HD 3200; Bandelin Electronic, Berlin, Germany) for 20 min at 30 W. The slides were washed by sonicating with distilled water and then dried at 100 °C. At this point, the glass substrates were coated by casting. For chemical characterisation, free films of the distinct sol-gel compositions were made by pouring 5 mL of each solution into non-stick Teflon molds. Finally, all the samples were heated for 2 h at 80 °C to cure the sol-gel. All the reagents were purchased from Sigma-Aldrich (St. Louis, MO, USA).

Table 1. Nomenclature of the designed sol-gel materials with the respective amounts of $CaCl_2$ and $MgCl_2$. The mass percentages are relative to the total amount of alkoxysilane.

Nomenclature	$CaCl_2$ (wt%)	$MgCl_2$ (wt%)
MT	0	0
Ca	0.5	0
Ca0.5Mg	0.5	0.5
Ca1Mg	0.5	1
Ca1.5Mg	0.5	1.5

2.2. Physicochemical characterisation

A solid-state silicon nuclear magnetic resonance spectroscope (^{29}Si-NMR; Bruker 400 Avance III WB Plus spectrometer, Billerica, MA, US), with a cross-polarization magic-angle spinning (CP-MAS) probe for solid samples, was used to study the cross-linking of the obtained sol-gel structures. The measurements were performed under the Bruker standard pulse sequence: 79.5 MHz frequency, 55 kHz spectral width, 2 ms contact time, and 5 s delay time. The spinning speed was 7.0 kHz. A Fourier transform infrared spectrometer (FTIR; Thermo Nicolet 6700, Thermo Fisher Scientific, NY, US) with an attenuated total reflection system (ATR) was employed to study the sol-gel materials. The spectra were recorded between 4000 and 400 cm^{-1}. A Bruker D4 Endeavor diffractometer (Bruker; Billerica, MA, USA) was employed to perform X-ray diffraction analysis (XRD). Measurements in the range of 5–70° (2θ) with a step size of 0.05°(2θ) and a scanning rate of 4 s $step^{-1}$ were made using filtered CuKα radiation (λ = 1.54 Å), an operating voltage of 40 kV and a filament current of 40 mA. The coatings applied onto Ti discs were morphologically characterised by employing a scanning electron microscope (SEM; Leica-Zeiss LEO, Leica, Wetzlar, Germany). The samples were sputtered with platinum before the evaluation to increase their conductivity. The sample roughness was measured with an optical profilometer PLm2300 (Sensofar, Barcelona, Spain). Three independent samples of each material were studied, and three measurements were performed for each sample. The results were expressed as the average values of Ra (arithmetic average roughness parameter). The sample wettability was obtained using an automatic contact angle meter OCA 20 (DataPhysics Instruments, Filderstadt, Germany). Ultrapure water drops (10 µL) were deposited on the discs at the speed of 27.5 µL s^{-1}. The drop angles were analysed using SCA 20 software (DataPhysics Instruments). Six samples were tested for each condition, and two drops were deposited on each of them. The hydrolytic degradation of the coatings was determined by examining mass loss during incubation in 50 mL of distilled water at 37 °C for 7, 14, 28, 42 and 56 days. The results are

displayed as mass loss percentages (%). Three distinct samples were used for each condition. The Mg^{2+} and Ca^{2+} release kinetics were characterised by employing an inductively coupled plasma atomic emission spectrometer (ICP-AES; Activa, Horiba Jobin Yvon IBH Ltd., Glasgow, UK). The coatings were incubated in ddH_2O at 37 °C for 28 days. After 2, 4, 6, 8, 24, 72, 168, 336, 504 and 672 h of incubation, 0.5-mL aliquots were analysed. Three individual samples were evaluated for each condition.

2.3. Evaluation of *in vitro* cell responses

2.3.1. Cell culture

Mouse calvaria osteosarcoma (MC3T3-E1) cell medium was composed of low-glucose DMEM (Gibco, Life Technologies, Thermo Fisher Scientific, NY, USA) supplemented with 1% penicillin/streptomycin (Gibco) and 10% FBS (Gibco). After 24 h, the culture medium was replaced with an osteogenic medium (DMEM, 1% of penicillin/streptomycin, 10% FBS, ascorbic acid (50 μg mL^{-1}) and 100 mM β-glycerol phosphate). The medium was changed every two days. Mouse murine macrophage (RAW 264.7) cell medium was composed of high-glucose DMEM (Gibco) supplemented with 1% penicillin/streptomycin and 10% FBS. Both cell lines were maintained in a cell incubator with 90% humidity and 5% CO_2 at 37 °C.

2.3.2. Biomaterial cytotoxicity

Cytotoxicity was assessed following the ISO 10993-5:2009 (Annex C) norm, and samples were prepared according to ISO 10993-12:2012. MC3T3-E1 cells were seeded into 96-well NUNC plates (Thermo Fisher Scientific) at 1×10^5 cells cm^{-2} and maintained in a humidified incubator. In parallel, the materials were incubated in a cell culture medium for serum extraction. After 24 h, the cells were exposed to the material extract for another day. The CellTiter 96® Proliferation Assay (MTS; Promega, Madison, WI) was used following the manufacturer's guidelines. The controls were the cells incubated without extract (negative control) and cells incubated with latex (positive control). The material was considered cytotoxic if the cell viability fell below 70%.

2.3.3. Cytoskeletal arrangement in osteoblasts

The MC3T3-E1 cells were seeded on the materials at 1×10^4 cells cm^{-2} to examine the changes in cytoskeleton arrangement. After 24 h, the samples were washed once with PBS and fixed with 4% paraformaldehyde (PFA) for 20 min at room temperature. Then, the samples were permeabilised with 0.1% Triton X-100 for 5 min and incubated with phalloidin (1:100; Abcam, Cambridge, UK) diluted in 0.1% w/v bovine serum albumin (BSA)-PBS for 1 h at room temperature. Nuclei were stained in a mounting medium with DAPI (Abcam). Fluorescence was recorded using a Leica TCS SP8 Confocal Laser Scanning Microscope with 20x (dry) lenses. The

obtained images were analysed employing the LAS X (Leica) and Image J tools (National Institutes of Health).

2.3.4. Alkaline phosphatase activity in osteoblasts

Cell mineralisation capability was evaluated by measuring the ALP activity, following the protocol of Araújo-Gomes *et al*. [22]. The MC3T3-E1 cells were seeded onto different surfaces in 48-well NUNC plates (Thermo Fisher Scientific) at 1.75 x 10^4 cells cm^{-2}. After culturing for 7 and 14 days, the cells were immersed in lysis buffer (0.2% Triton X-100, 10 mM Tris-HCl, pH 7.2) for 10 min at 4 °C. Then, 100 µL of *p*-NPP (1 mg mL^{-1}) in substrate buffer (50 mM glycine, 1 mM $MgCl_2$, pH 10.5) was added to 100 µL of the sample. After 2 h of incubation in the dark, the absorbance at 405 nm was measured using a microplate reader. Alkaline phosphatase activity was obtained from the standard curve for *p*-nitrophenol in 0.02 mM sodium hydroxide and normalised to protein content (determined employing a Pierce BCA assay kit; Thermo Fisher Scientific).

2.3.5. Cytokine secretion in macrophages

The effect of the materials on the secretion of pro- and anti-inflammatory cytokines was examined by analysing the cell culture medium obtained after incubation of RAW264.7 cells. The medium was collected and frozen until further analysis. Tumour necrosis factor (TNF)-α and transforming growth factor (TGF)-β concentrations were determined using an ELISA (Invitrogen, Thermo Fisher Scientific) kit, according to the manufacturer's instructions.

2.3.6. Relative gene expression: RNA extraction, cDNA synthesis and qRT-PCR

For RNA extraction, MC3T3-E1 cells were grown for 7 and 14 days at density of 1.75 × 10^4 cells cm^{-2} for 7 and 14 days. The RAW264.7 cells were seeded at the density of 30 × 10^4 cm^{-2} and cultured for 2 and 4 days. The assays were carried out in 48-well NUNC plates. At each time point, RNA was extracted with TRIzol following the protocol by Cerqueira *et al*. [23]. The RNA concentration, integrity and quality were measured using NanoVue® Plus Spectrophotometer (GE Healthcare Life Sciences, Little Chalfont, UK). For cDNA synthesis, approximately 1 µg of total RNA was converted into cDNA using PrimeScript RT Reagent Kit (Perfect Real Time; TAKARA Bio Inc., Shiga, Japan). The reaction was carried out under the following conditions: 37 °C for 15 min, 85 °C for 5 s and a final hold at 4 °C. The resulting cDNA was diluted in DNase-free water to a concentration suitable for gene expression evaluation. Quantitative real-time PCRs (qRT-PCR) were carried out in 96-well plates (Applied Biosystems®, Thermo Fisher Scientific). Primers for each gene were designed using the Primer3Plus software tool on the basis of specific NCBI DNA sequences and purchased from Thermo Fischer Scientific. Targets studied for each cell line are

shown in **Supplementary Table 1**. Each reaction mix contained 1 µL of cDNA, 0.2 µL of specific primers (forward and reverse at the concentration of 10 µM L^{-1}) and 5 µL of SYBR Premix Ex Taq (Tli RNase H Plus; TAKARA) in a final volume of 10 µL. Reactions were carried out in a StepOnePlus™ Real-Time PCR System (Applied Biosystems®). Fold changes were calculated using the $2^{-\Delta\Delta Ct}$ method.

2.4. Proteomic analysis of the adsorbed protein layer

The protocol described by Romero-Gavilán *et al.* [17] was followed for the proteomic analysis of the adsorbed protein layer. The materials were incubated for 3 h (37 °C, 5% CO_2) in 24-well NUNC plates (Thermo Fisher Scientific) with 1 mL of human serum from male AB plasma (Sigma–Aldrich). Then, to eliminate non-adsorbed proteins, the materials were washed five times with ddH_2O and once with wash buffer (100 mM NaCl, 50 mM Tris–HCl, pH 7.0). The adsorbed proteins were extracted in a buffer containing 2M thiourea, 7M urea, 4% CHAPS and 200 mM DTT. Four independent replicates of each surface were analysed; each replicate was made by pooling the extract of proteins adsorbed onto four discs. Total protein concentration in the serum was obtained employing a Pierce BCA assay kit (Thermo Fisher). The analysis of the proteins was performed using electrospray tandem mass spectrometry, employing a nanoACQUITY UPLC (Waters, Milford, MA, USA) coupled to an Orbitrap XL (Thermo Electron, Bremen, Germany) as described by Romero-Gavilán *et al.* [24]. Each sample was analysed in a quadruplicate. Differential protein analysis was carried out using PEAKS (Bioinformatics Solutions Inc., Waterloo, Canada).

2.5. Statistical analysis

For physicochemical characterisation and *in vitro* assay data, considering normal distribution and equal variance, one-way variance analysis (ANOVA) with Tukey post hoc test was performed. The student's *t*-test was conducted after the ANOVA analysis to confirm the results. Data are expressed as means ± standard error (SE). Statistical analysis was performed using GraphPad Prism 5.04 software (GraphPad Software Inc., La Jolla, CA, USA) and considered significant at $p \leq 0.05$. To understand the effects of Ca and CaMg mixtures, comparisons between MT (without any ion) and MT ion-doped were made. The asterisk (*) indicates differences between the MT and ion-doped coatings, and the rhombus (◆), the differences between the Ca-doped and CaMg-doped materials. Regarding proteomic data analysis, Student's *t*-test was conducted to evaluate differences between MT and MT with added Ca and CaMg using Progenesis software. The changes in protein adsorption were considered statistically significant at both $p \leq 0.05$ and abundance ratio between conditions of more than 1.5 in either direction (higher or lower).

3. Results

3.1. Physicochemical characterisation

The different materials were chemically analysed using FTIR, ^{29}Si-NMR and XRD (**Figure 1**). **Figure 1a** shows the FTIR spectra for each material. The spectra did not show significant changes for materials with added $CaCl_2$ or $CaCl_2$ and $MgCl_2$ in comparison with the base material MT. The bands related to the polysiloxane chain vibration (770, 1020, and 1125 cm^{-1}) indicate the correct formation of Si-O-Si bonds [25]. The band at 950 cm^{-1} is associated with Si-OH bonds, characteristic for non-condensed groups [25] . Bands at 1265 and 2980 cm^{-1}, associated with the Si-C and C-H bonds, respectively [26], reflect the methyl group integrity in the sol-gel structure after the synthesis process. Similarly, incorporating calcium and magnesium salts did not significantly affect the ^{29}Si-NMR spectra (**Figure 1b**). The characteristic signals of the MTMOS trifunctional precursor (T units - $CH_3{\cdot}SiO_3$) were detected in the -50 and -75 ppm range, while the signals of the TEOS tetrafunctional precursor (Q units - SiO_4) were seen between -97.5 and -120 ppm [26]. Peaks at -62 and -70 ppm are associated with T^2 and T^3 species formation in the network, while peaks at -99, -106, and -116 ppm represent Q^2, Q^3 and Q^4 reticulated structures, respectively [25]. All compositions attained a proper cross-linking degree as T^3 was the highest chemical shift in MTMOS and Q^3 in TEOS. Moreover, non-condensed species (T^0 and Q^0) and structures with only one condensed bond (T^1 and Q^1) were not detected. **Figure 1c** shows the XRD patterns obtained for the different formulations. These results prove the amorphous nature of the synthesised materials as no peaks associated with the formation of Ca or Mg-related crystalline structures were observed. No significant differences were found between the distinct compositions. The diffraction peak at 10° (2θ) can be associated with the presence of incompletely hydrolysed precursors, and the broad peak at 21° (2θ) is characteristic of the SiO_2 amorphous sol-gel network [27].

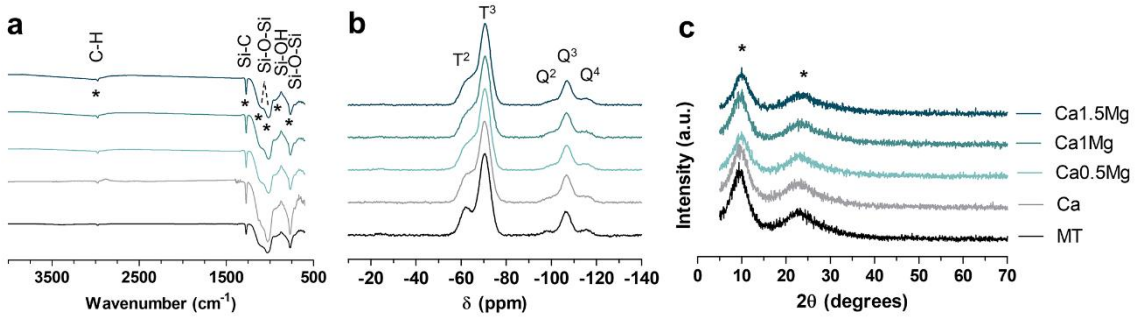

Figure 1. (a) FTIR, (b) ^{29}Si-NMR spectra and (c) XRD of the obtained sol-gel materials.

The synthesised sol-gel materials were applied as coatings onto Ti discs. The resulting coatings entirely covered the Ti surface, as shown in **Figure 2**. Contact angle measurements were carried

out to evaluate changes in surface wettability after the addition of Ca^{2+} and Mg^{2+} (**Figure 2a**). The material with 0.5% $CaCl_2$ in the sol-gel network had significantly increased contact angle to values between 50° and 75°. The materials containing both Ca and Mg ions showed greater contact angles than the MT and Ca materials. However, increasing the amount of added $MgCl_2$ did not cause further significant changes in the wettability of the coatings.

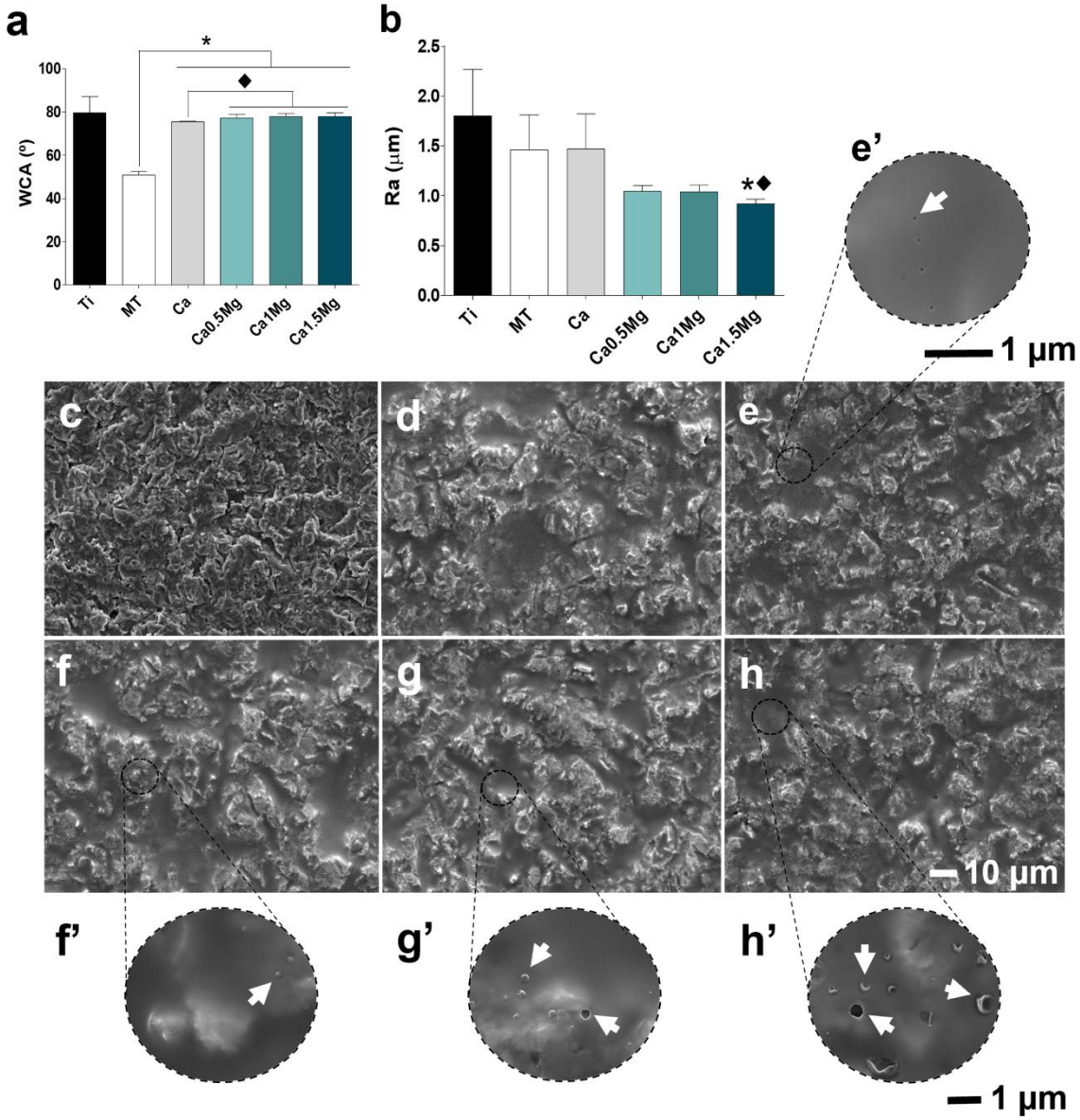

Figure 2. Contact angle (WCA, a) and roughness (Ra, b) results. Data are shown as means ± SD. The asterisk (*) indicates differences between the MT and the ion doped-coatings, and the rhombus (◆), differences between the Ca-doped and the CaMg-doped materials. SEM microphotographs of (c) Ti, (d) MT, (e) Ca, (f) Ca0.5Mg, (g) Ca1Mg, (h) Ca1.5Mg and (e´–h´) the enlarged images. White arrows point to examples of pinholes and bubbles detected in the coatings. Scale bars: (c–h) 10 and (e'–h') 1 µm.

Figure 2b shows the effects of Ca and Mg on the coating roughness. The values of Ra decreased for coated samples in comparison with non-coated discs. No differences between roughness values of MT and Ca coatings were observed. In contrast, Ca0.5Mg, Ca1Mg and Ca1.5Mg coatings showed significantly reduced Ra in comparison with MT and Ca. The roughness data were consistent with the results of SEM analysis. The sol-gel tended to accumulate in the cavities of the initial Ti roughness, decreasing the Ra (**Figure 2c-h**). Adding 0.5% $CaCl_2$ to the coating caused the appearance of small pores, about 45 nm in diameter, not observed in the base MT material (**Figure 2e'**). Raising the content of Mg increased these irregularities; small bubbles and pores were observed (**Figure 2f'-h'**). Moreover, they became larger as more $MgCl_2$ was incorporated, up to 0.5-µm diameter in the Ca1.5Mg (**Figure 2h'**). No salt precipitates were observed.

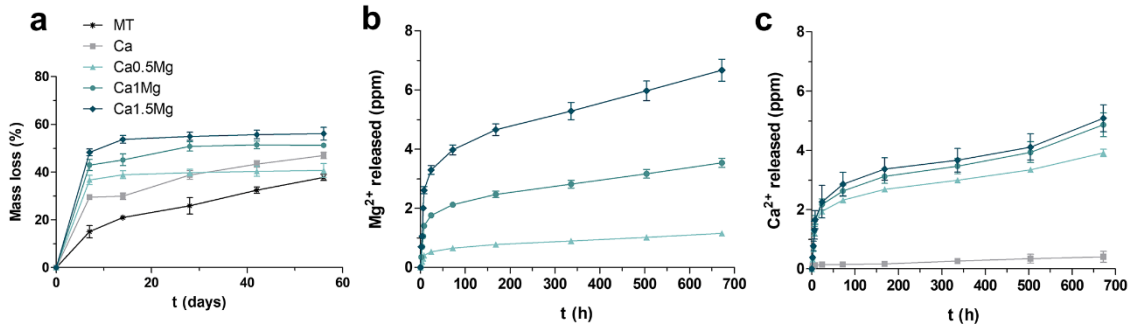

Figure 3. Hydrolytic degradation (a). Kinetic release of Mg^{2+} (b) and Ca^{2+} (c) ions from the developed sol-gel coatings. Data are shown as means ± SE.

Figure 3a shows the mass loss for all coated samples versus time. In general, the degradation by hydrolysis was fastest during the first week of incubation. After this period, the sol-gel coatings continue to degrade throughout the assay at a low speed. Adding Ca to the MT network slightly increases the degradability. The mass losses were from 37.8% for MT to 47.0% for Ca material after 56 days of testing. The kinetics of degradation for the Ca0.5Mg and the Ca coatings were similar. However, the sol-gel network showed larger weight losses when more $MgCl_2$ was added. Thus, the mass lost after 56 days from Ca1Mg and Ca1.5Mg coatings was 51.3 and 56.1%, respectively. **Figures 3b** and **c** show the kinetic liberation of Mg^{+2} and Ca^{2+} ions. A continuous release of Mg^{2+} was observed throughout the assay, being this liberation faster during the first 24 h (**Figure 3b**). As expected, the more $MgCl_2$ was incorporated into the material, the more Mg^{2+} was released. The maximum release of this ion, 6.67 ppm of Mg^{2+}, was observed for the Ca1.5Mg sample after 672 h of incubation. Similarly, Ca^{2+} was liberated throughout the test (**Figure 3c**), and the release kinetics was higher during the first day of incubation. Although the Ca concentration is the same in all the developed materials, the release of this cation is

significantly higher for coatings with both Ca and Mg than for the coating only doped with Ca. Moreover, the amount of Ca^{2+} liberated increased as more $MgCl_2$ was added to the network, reaching 5.08 ppm of Ca^{2+}, the maximum concentration detected in the assay (Ca1.5Mg; 672 h).

3.2. *In vitro* cell responses

3.2.1. Cytotoxicity, cytoskeleton arrangement and ALP activity

Our tests showed that none of the materials analysed in this study was cytotoxic (**Supplementary Figure 1**). In addition, all the coatings showed the same level of cell viability. To evaluate the effects of the materials on the arrangement of the cellular cytoskeleton, the cells were stained with phalloidin after 1-day incubation (**Figure 4a–f**). Cells cultured on Ti and MT showed a triangular shape with few lamellipodia (**Figure 4a–b**). Those grown on Ca, Ca0.5Mg and Ca1Mg coatings had a more elongated shape with protruding lamellipodia and filopodia (white arrows; **Figure 4b–e**). The cells cultured on Ca1.5Mg also had lamellipodia; however, the cell shape was generally less elongated (**Figure 4f**). Exposure to Ca, Ca0.5Mg and Ca1Mg materials significantly increased the cell surface area in comparison with cells exposed to MT (**Figure 4g**).

To understand the effects of the materials on mineralisation capability, the ALP activity was examined (**Figure 4h**). At 7 days, there was a significant increase in ALP activity in cells grown on Ca and Ca1.5Mg materials in comparison with MT. In contrast, the cells cultured with Ca0.5Mg and Ca1Mg showed lower ALP activity than those grown with Ca biomaterial. After 14 days, all these cultures showed a significant decrease in ALP activity in comparison with cells exposed to MT.

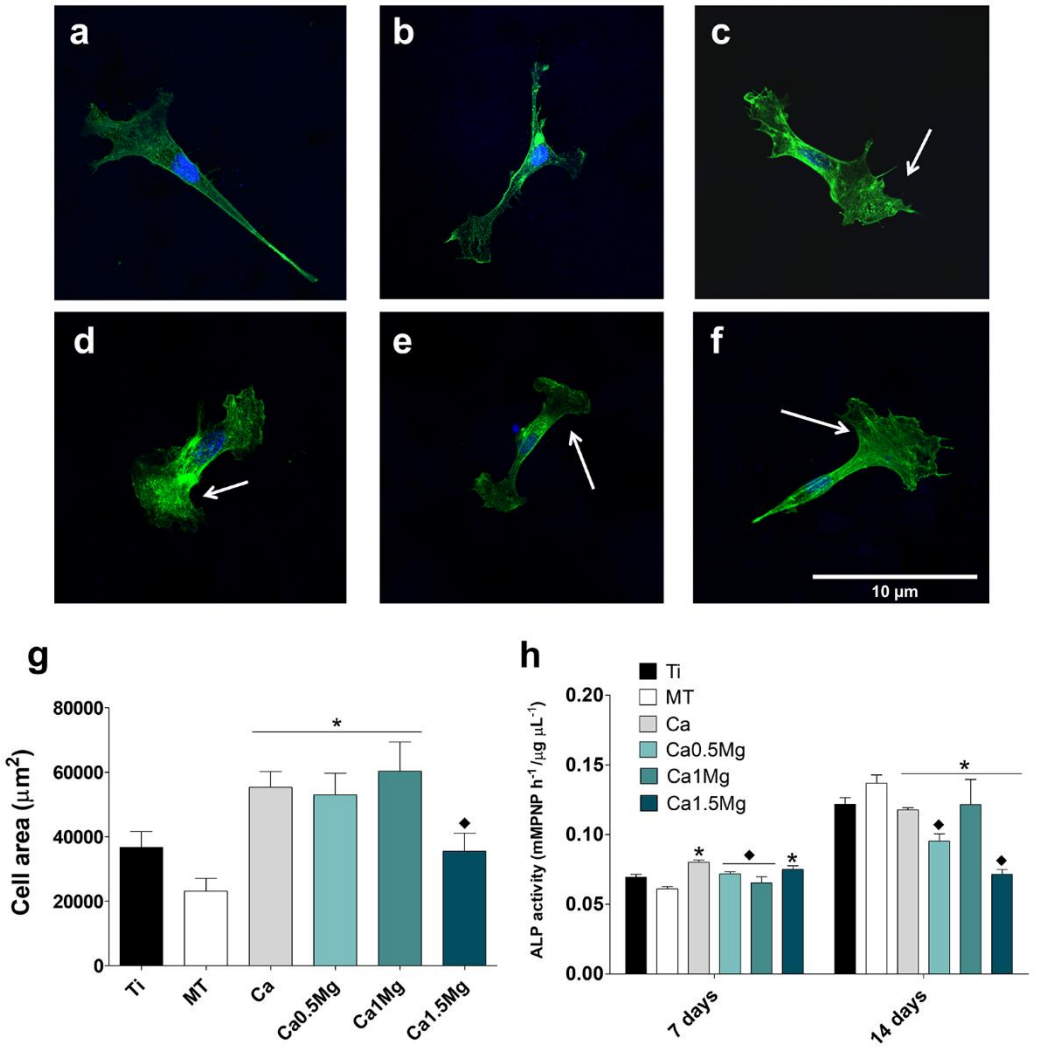

Figure 4. Confocal fluorescence microscopy images of cytoskeleton arrangement of MC3T3-E1 cultured on (a) Ti, (b) MT, (c) Ca, (d) Ca0.5Mg, (e) Ca1Mg and (f) Ca1.5Mg. The area of the cells adhering to the materials (g). Actin was stained with phalloidin (green) and nuclei with DAPI (blue). White arrows point the lamellipodia and filopodia. Scale bar: 10 µm. ALP activity (h) in MC3T3-E1 after 7 and 14 days. The results are shown as means ± SE. The asterisk (*) indicates differences between the MT and the ion-doped coatings, and the rhombus (◆) indicates differences between the Ca-doped and the CaMg-doped materials.

3.2.2. Cytokine secretion in macrophages

Cytokine secretion in the RAW264.7 cell culture medium was measured to evaluate the effects of the ion-doped materials on inflammation. The levels of anti-inflammatory cytokine TGF-β only showed a significant increase relative to MT in Ca0.5Mg after 2 days (**Figure 5a**). However, after 4 days, all CaMg materials were associated with significantly higher secretion of this cytokine in comparison with both MT and Ca cultures. The secretion of pro-inflammatory cytokine TNF-α was significantly reduced in Ca-exposed cells in comparison with MT after 2 days (**Figure 5b**). At

the same time, increased secretion of this cytokine was observed for cells cultured with Ca1.5Mg. After 4 days, the cells exposed to all CaMg materials secreted more TNF-α than those grown with MT or Ca coatings (**Figure 5b**).

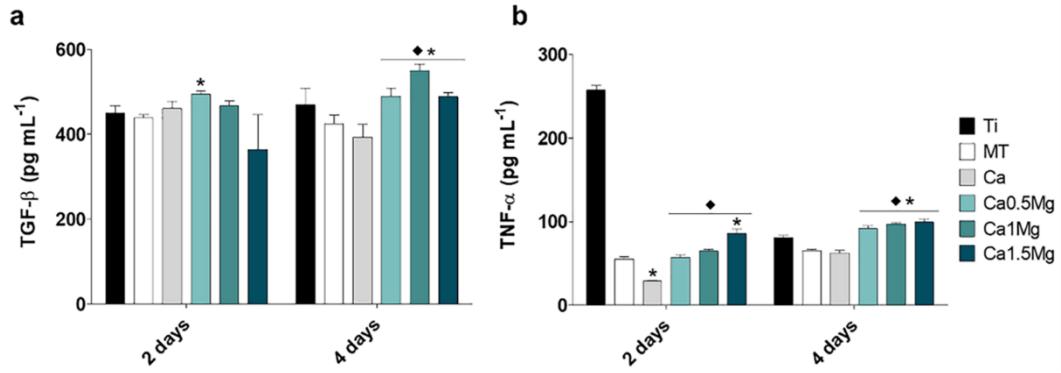

Figure 5. Cytokine secretion quantification using ELISA of (a) TGF-β and (b) TNF-α for RAW264.7 cells after 2 and 4 days of culture. Results are shown as means ± SE. The asterisk (*) indicates differences between MT and the ion-doped coatings, and the rhombus (◆) indicates differences between the Ca-doped and the CaMg-doped materials.

3.2.3. Relative gene expression

The expression of several genes was examined to understand better the effects of the materials on osteogenesis (genes for ALP, TGF-β, SP7 and RUNX2) and inflammatory responses (genes for TNF-α, IL-1β, TGF-β and IL-10). After 7 and 14 days, the Ca0.5Mg cultures showed significantly higher expression of ALP than the MT and Ca cultures (**Figure 6a**). Similarly, Ca0.5Mg and Ca1.5Mg biomaterials increased the expression of SP7 after 7 days of incubation. However, the fold change was significantly lower for Ca0.5Mg-exposed cells after 14 days, while it was augmented in Ca, Ca1Mg and Ca1.5Mg cultures (**Figure 6b**). The *TGF-β* expression increased after a 7-day incubation with Ca0.5Mg but decreased significantly after 14 days for all the materials except Ca (**Figure 6c**). The RUNX2 expression was unchanged after 7 days. However, after 14 days, the expression of this gene was higher in Ca-exposed cells than in MT cultures and significantly lower in the cells incubated with CaMg materials than in cells cultured with the Ca coating (**Figure 6d**).

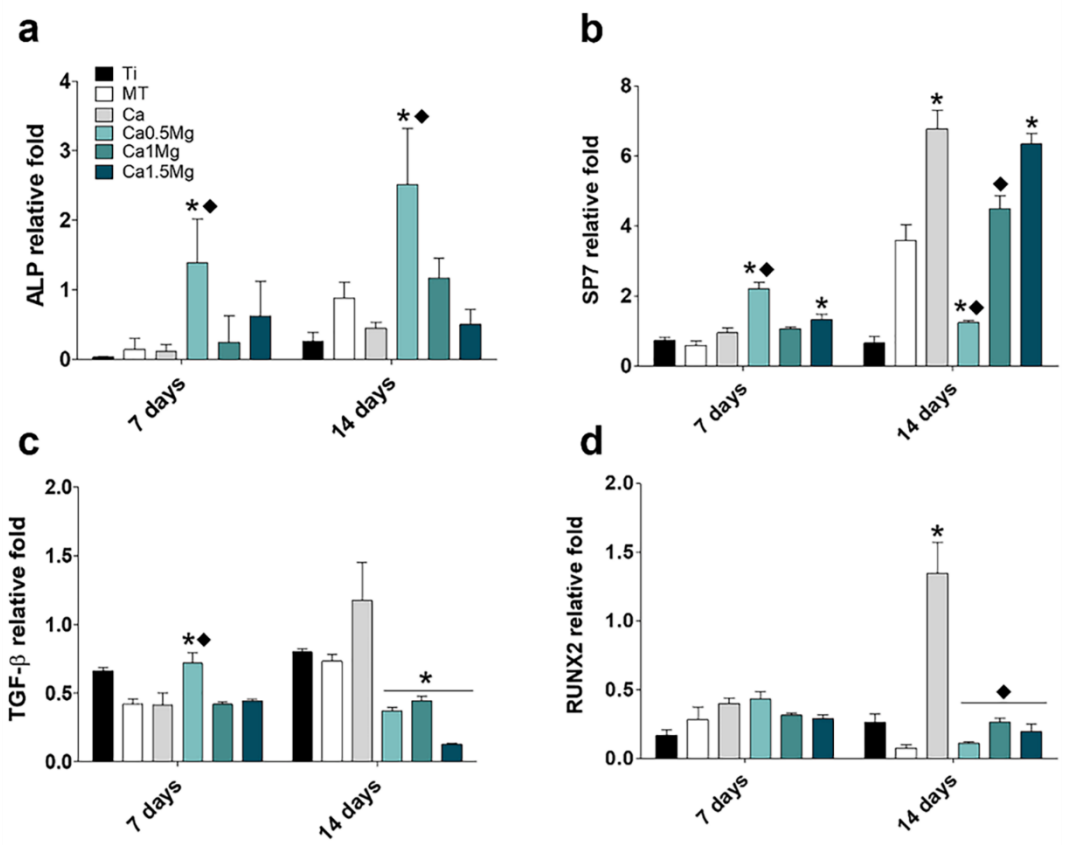

Figure 6. Relative gene expression of (a) alkaline phosphatase (*ALP*), (b) transcription factor SP7/osterix (*SP7*), (c) transforming growth factor (*TGF-β)* and (d) runt-related transcription factor 2 (*RUNX2*) in MC3T3-E1 at 7 and 14 days. Data were normalised to blank samples (wells without any biomaterial) using the $2^{-\Delta\Delta Ct}$ method. Results are shown as means ± SE. The asterisk (*) indicates differences between MT and the ion-doped coatings, and the rhombus (◆) indicates differences between the Ca-doped and the CaMg-doped materials.

The analysis of the expression of genes related to inflammatory responses showed that TNF-α gene expression was significantly reduced in Ca1Mg and Ca1.5Mg cultures in comparison with cells grown with the Ca material (**Figure 7a**) after 2 days. After 4 days, cultures with all materials containing Ca (Ca-only or Ca-Mg mixtures) increased the expression of this gene in comparison with MT. Cells exposed to Ca0.5Mg also showed an increased expression of TNF-α in comparison with Ca cultures. After 2 days of incubation with Ca, the expression of the gene (**Figure 7b**) decreased in comparison with MT cultures. In contrast, its expression in the cells exposed to Ca0.5Mg was significantly higher than in cells grown with the Ca material. After 4 days, Ca1Mg and Ca1.5Mg increased the *IL-1*β expression with respect to MT.

After 2 days, the levels of anti-inflammatory marker increased in Ca1Mg cultures in comparison with MT, and its expression was significantly lower after incubation with Ca0.5Mg than with Ca

material (**Figure 7c**). However, CaMg coatings increased the TGF-β expression with respect to MT and Ca after 4 days of culture. Lastly, the *IL-10* gene (**Figure 7d**) showed higher expression in Ca0.5Mg than in MT cultures (at 2 days). The expression of this gene in cells incubated with Ca1Mg was significantly increased, while with Ca1.5Mg was reduced with respect Ca at the same time point. On the fourth day of assay, the *IL-10* expression significantly decreased in all the cultures with Ca-containing materials (irrespective of their Mg content) in comparison with the MT cultures. The cells exposed to Ca1Mg and Ca1.5Mg also showed lower expression of this marker than the cells grown on the Ca material.

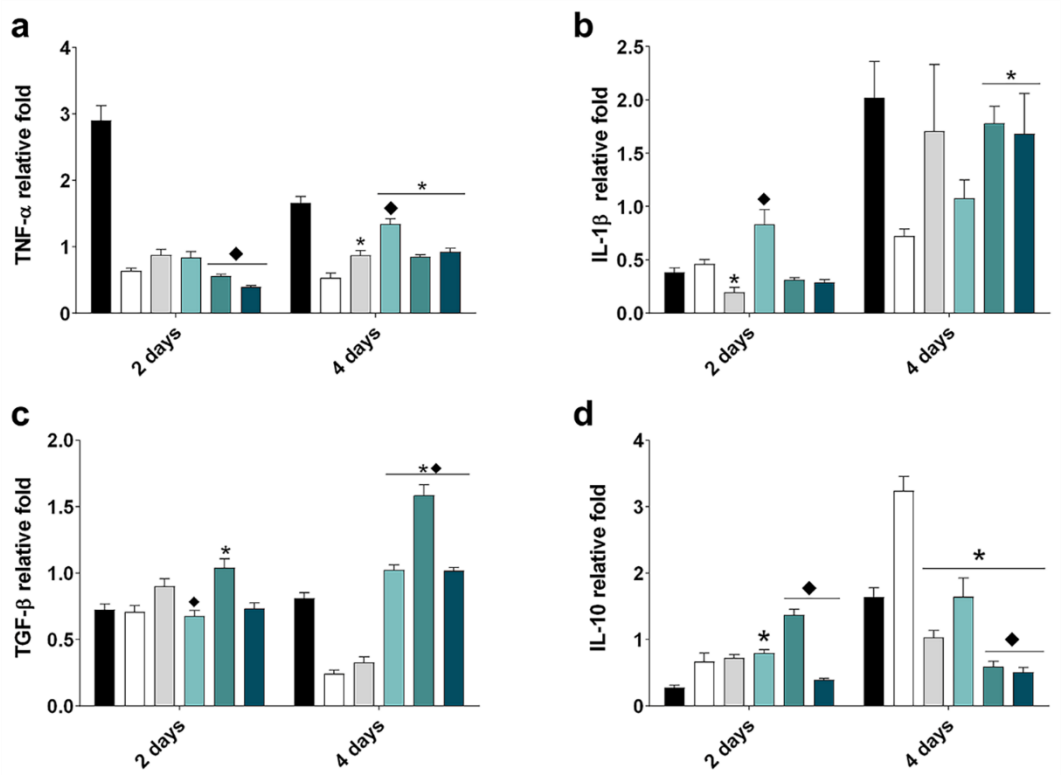

Figure 7. Relative gene expression of (a) tumour necrosis factor (*TNF*)-α, (b) interleukin (*IL-1β*), (c) transforming growth factor (*TGF*)-β and (d) *IL-10* on RAW264.7 after 2 and 4 days. Data were normalised to blank samples (wells without any biomaterial) using the $2^{-\Delta\Delta Ct}$ method. Results are shown as means ± SE. The asterisk (*) indicates differences between MT and the ion-doped coatings, and the rhombus (◆) indicates differences between the Ca-doped and the CaMg-doped materials.

3.3. Proteomic analysis

The nLC-MS/MS analysis of eluted proteins identified 84 proteins differentially adsorbed onto the CaMg materials in comparison with the MT base material (**Supplementary Table 2**). **Table 2** summarises the differentially adsorbed proteins found on the Ca and CaMg materials with biological functions key for bone tissue regeneration. Among these, 16 proteins related to

inflammatory responses, particularly the complement system activation (CO6, CO5, CO4B, CO4B and CO9) and its regulation (CFAH and VTDB), showed increased affinity to CaMg surfaces. Proteins with roles in the acute inflammatory responses (A1AG1, A1AG2 and AACT), immune system regulation (PIGR, PIP) and innate immune mediation (HPTR, HPT) were prevalent on CaMg surfaces. The ITIH2 protein, associated with the localisation, synthesis and degradation of hyaluronan, was also preferentially adsorbed on these surfaces. CRP, a positive acute-phase protein, was more abundant on Ca and Ca1Mg materials. Seven proteins associated with coagulation (HRG, HBA, ZPI, HEP2 and A2MG) and cell adhesion (FBLN1 and HABP2) showed increased affinity to CaMg materials. Some other proteins with functions in cell adhesion (ZA2G, LG3BP, DSG1 and DESP), tissue regeneration processes (CLUS and TSK) and several apolipoproteins (APOF, APOL1, APOA4, APOH, APOM and APOA1) were also preferentially adsorbed on these surfaces. In contrast, the protein layer formed on these materials contained a reduced proportion of 14 proteins associated with coagulation (PROS, THRB, KNG1, IPSP, FA11, PFAV, CXCL7, ANT3, FA10, PLF4, FA9, FA12, PROC and CBPB2). The amounts of immunoglobulins (KVD40, IGKC, IGHG2, KV127, HV118 and KV106) and FHR5 (associated with complement system regulation) were also reduced. Similarly, the adsorption levels of two proteins associated with inflammatory responses (MASP2 and FCN2), a protein associated with cell adhesion (PKP1) and two apolipoproteins (APOC4 and APOE) were diminished. Finally, three proteins associated with the cartilage structure (COMP, PCOC1 and PRG4) and two involved in the tissue regeneration process (VTNC and IBP4) were also less abundant on the CaMg materials than on the MT.

Table 2. Proteins differentially adsorbed onto the sol-gel materials doped with Ca or Ca and Mg and their associated biological processes (immune response, cell adhesion, tissue regeneration and coagulation).

Biological process		Ca/MT	Ca0.5Mg/MT	Ca1Mg/MT	Ca1.5Mg/MT
Immune responses	Increased adsorption	PIGR CO6 CO5 CO4B A1AG1 ITIH2 CO9 VTDB ALBU AACT HPT CFAH A1AG2 IGHM ITIH1 HEMO IGHG4 CRP	PIGR CO6 PIP CO5 CO4B CO4A A1AG2	PIGR CO6 PIP CO5 CO4B CO4A ITIH2 CO9 VTDB HPTR AACT HPT A1AG2 ALBU ITIH1 HEMO	PIGR CO6 PIP CO5 CO4B CO4A ITIH2 CO9 HPTR AACT HPT CFAH ALBU
	Reduced adsorption	KVD40 IGKC MASP2 KV127 KV106 FHR5 PRG4	KV320 KVD40 IGKC MASP2 IGHG2 KV127 HV118 KV106 FHR5 FCN2 BLMH	KVD40 MASP2 IGHG2 KV106 FHR5 FCN2 BLMH	MASP2 IGHG2 KV127 HV118 KV106 FHR5 FCN2 BLMH
Tissue regeneration	Increased adsorption	CLUS	CLUS	CLUS	TSK CLUS
	Reduced adsorption	COMP PCOC1 VTNC IBP4 PRG4	COMP PCOC1 VTNC IBP4 PRG4	COMP PCOC1 VTNC IBP4 PRG4	COMP PCOC1 VTNC IBP4 PRG4
Cell adhesion	Increased adsorption	LG3BP DSG1 FBLN1 DESP HABP2	ZA2G LG3BP DSG1 DESP	ZA2G LG3BP DSG1 FBLN1 HABP2	ZA2G LG3BP DSG1 FBLN1 DESP HABP2

	Reduced adsorption	PKP1	PKP1	PKP1	
Coagulation	Increased adsorption	HBA ZPI HABP2 A2MG	HRG HBA ZPI F13B	HRG HBA ZPI HABP2 HEP2 A2MG F13B	HRG HBA ZPI HABP2 HEP2 A2MG
	Reduced adsorption	HRG PLMN THRB KNG1 IPSP FA11 ANT3 FA10 PLF4 FA9 FA12 PROC CBPB2	PROS THRB KNG1 IPSP FA11 PF4V CXCL7 ANT3 FA10 PLF4 FA9 FA12 PROC CBPB2	PROS THRB KNG1 IPSP FA11 PF4V CXCL7 ANT3 FA10 PLF4 FA9 FA12 PROC CBPB2	PROS THRB KNG1 IPSP FA11 PF4V CXCL7 ANT3 FA10 PLF4 FA9 FA12 PROC CBPB2

A comparison between Ca and CaMg materials was performed to further understand the effect of doping mixtures. Seventeen proteins were preferentially more adsorbed to the CaMg surfaces (**Supplementary Table 3**). Of these, five were associated with coagulation (HRG, SPB12, PLMN, HBA and FA12), one related to inflammatory responses (PIP), and one was an apolipoprotein (APOA4). Another, the PLAK protein, was associated with cell adhesion. In contrast, the TSK protein and HV551, CO8B, BLMH and CRP proteins, linked to immune responses, were significantly less adsorbed on the CaMg than on Ca surfaces. **Figure 8** shows the effect of mixtures on the adsorption of the most relevant proteins. The abundance of HRP, SPB12, PLMN and HBA proteins increased with increasing concentration of Mg (**Figure 8a, b, c, and d**). However, no differences in FA12 levels were found for Ca, Ca0.5Mg and Ca1.5Mg coatings (**Figure 8e**). Among the proteins related to inflammatory responses, the adsorption of CRP significantly decreased on Ca1.5Mg (**Figure 8f**), while Ca0.5Mg and Ca1Mg materials adsorbed less CO8B (**Figure 8g**) and BLMH (**Figure 8h**), respectively.

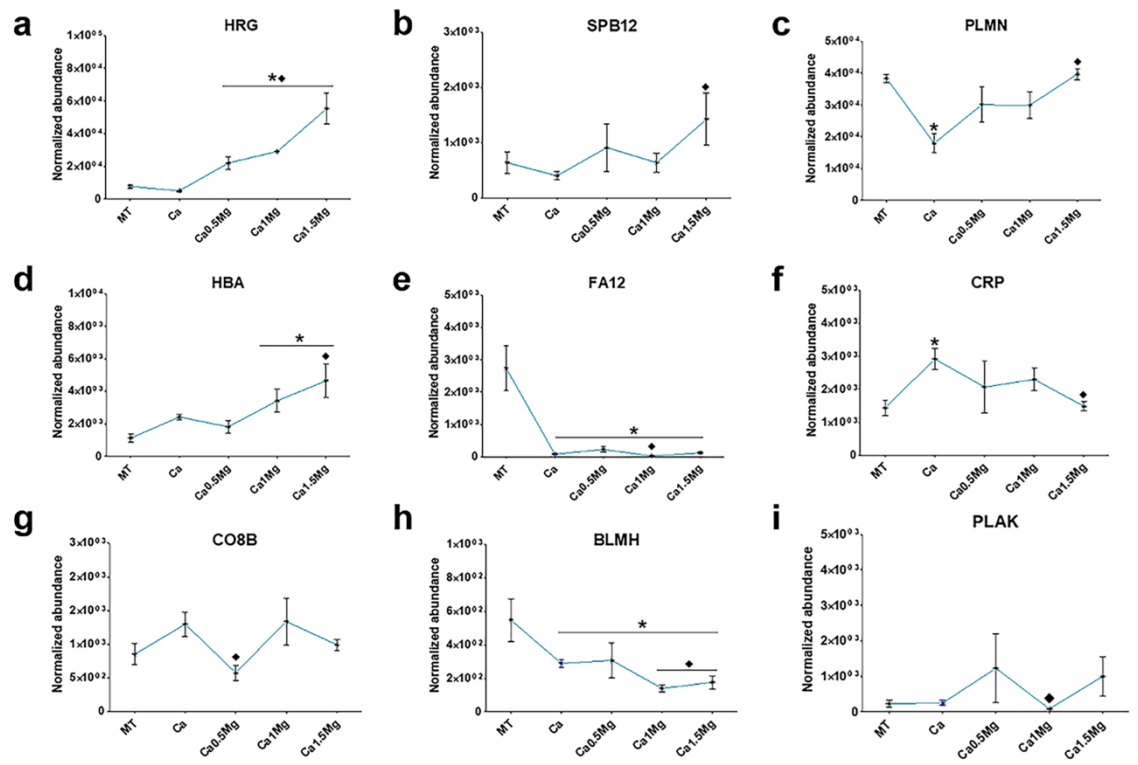

Figure 8. Normalised abundance of proteins linked to various biological processes, adhering to different materials. The proteins associated with coagulation: (a) histidine-rich glycoprotein (HRG), (b) serpin B12 (SBP12), (c) plasminogen (PLMN), (d) haemoglobin subunit alpha and (e) coagulation factor XII (FA12). Associated with immune responses: (f) C-reactive protein (CRP), (g) complement component C8 beta chain (CO8B) and bleomycin hydrolase (BLMH). Associated with cell adhesion: (i) junction plakoglobin (PLAK). Results are shown as means ± SE. The asterisk (*) indicates differences between MT and the ion-doped coatings, and the rhombus (◆) indicates differences between the Ca-doped and the CaMg-doped materials.

4. Discussion

Calcium and magnesium are important in biological systems, particularly in the bone tissue and the associated processes, such as inflammation or coagulation. The individual effects of these two ions on the protein adsorption on implant surfaces have been already examined [10,20]. It has been shown that Ca has a high affinity to proteins involved in coagulation and inflammatory responses, while the addition of Mg increases the material affinity to proteins related to cell adhesion. With these data in mind, designing and analysing a biomaterial to combine the regulatory properties of the two ions was a promising path to follow. Thus, the main aim of this study was to develop and characterise a new coating enriched with mixtures of Ca and Mg salts. Even though the sol-gel coating bioactivity and the SAE-Ti substrate itself can have an effect on the biological responses, the comparison between Ca and CaMg doped coatings to MT (without

any ion) should improve the understanding of the effect on protein adsorption patterns and *in vitro* cell responses of CaMg combination.

As the ^{29}Si-solid NMR showed, the incorporation of $CaCl_2$ and $MgCl_2$ into the sol-gel network did not affect the final silica network cross-linking. The presence of separated phases enriched with Ca or Mg in the network would suppose the presence of heterogeneity in the cations distribution on the coating. However, no crystalline structures were found on the materials; Ca^{2+} and Mg^{2+} were likely trapped in the hybrid cross-linked structure by hydrogen bonding, Van der Waals or electrostatic forces [28]. The $CaCl_2$ incorporation into the sol-gel network led to a significant increase in the contact angle and changes in the surface roughness. Romero-Gavilán *et al.* [20] have reported that incorporating 0.5% of $CaCl_2$ into a sol-gel network does not significantly change the material roughness but increases the contact angle. The incorporation of the CaMg mixture did not affect the final network either. However, it led to a significant decrease only in roughness for Ca1.5Mg, probably due to the increased viscosity of the sol-gel mixture caused by the greater amounts of added salts. Roughness offers an effective surface for bone implant contact and cell proliferation. Jemat *et al.* [29] reported that surface roughness ranging from 0.44 to 8.68 µm provides a good substrate for osseointegration. Despite the reduction observed in Ra, all values obtained in the materials studied vary between 1.79 and 0.91 µm, thus making these surfaces optimal from this point of view. The ion release experiment revealed that the more $MgCl_2$ was added to the network, the more Mg^{2+} and Ca^{2+} ions were released. Although the amount of Ca added is constant, as more $MgCl_2$ was added to the network, more mass was lost during the coating degradation; consequently, more Ca^{2+} was released from the CaMg than Ca material. The materials with Ca and the mixtures of Ca and Mg formed small pores observed on the SEM microphotographs. These pores could allow water to enter the network, increasing its degradation and Mg^{2+} and Ca^{2+} release and decreasing the barrier effect of the coating. The release kinetics were stable for 30 days (the end of the assay), reaching 6 ppm of Mg^{2+} and about 5 ppm of Ca^{2+} for the material with the highest concentration of both ions (Ca1.5Mg). As Mg is non-cytotoxic at concentrations as high as 10 mM [30] and Ca at concentrations up to 150 ppm [31], this explains the lack of cytotoxicity of the obtained coatings.

Upon the implantation, nonspecific protein adsorption onto the material surface occurs nearly instantaneously [16]. This phenomenon plays a major role in determining the subsequent interactions between implants and tissues. Its thorough analysis is essential for understanding the cell responses and improving the design of biomaterials [15]. Here, we examined the protein layer formed on the biomaterials during incubation with human serum. The nLC-MS/MS analysis identified 84 proteins differentially adsorbed onto the CaMg surfaces compared to MT. Five of the proteins preferentially adsorbed onto the CaMg materials are associated with the

complement system activation (CO6, CO5, CO4B, CO4B and CO9). The complement system is an important effector of innate immunity, participating in the opsonization of foreign bodies [32]. However, once activated, the system needs to be tightly controlled as an excessive reaction can lead to severe inflammation and cell damage [33]. Three proteins associated with the regulation of the process (CFAH, VTDB and CLUS) showed increased affinity to CaMg surfaces in an added cation- dose-dependent manner. Complement factor H (CFAH) is a critical regulator of the alternative complement pathway. It is associated with maintaining the balance between osteoblasts and osteoclasts and the resulting bone tissue quality [33,34]. Vitamin D binding protein (VTDB) plays a major role in transporting vitamin D metabolites. It has been implicated in enhancing the complement C5 system in association with annexin A2 [35]. Moreover, the VTDB stimulates reactive oxygen intermediates (ROIs) and cellular debris ingestion, leading to macrophage activation [36]. The apolipoprotein clusterin (CLUS) regulates the complement proteins C6, C7, C8 and C9 and the membrane attack complex (MAC) formation. CLUS also regulates the NF-κB pathway and reduces apoptosis and oxidative stress in immune cells [37].

Seven other apolipoproteins (APOF, APOL1, APOA4, APOH, APOM and APOA1) showed increased affinity to CaMg surfaces. These proteins are also involved in regulating the complement system [38] and lipid metabolism. In contrast, the absorption of ficolin-2 (FCN2), known to activate the lectin pathway of complement activation [39], was weaker on the CaMg than on MT material.

Normal immune responses involve immune complexes formed by specific immunoglobulins with target antigens, facilitating the clearance or neutralisation of foreign bodies [40]. The CaMg coatings significantly decreased the adsorption of this protein type (IGH2, KV127, HV118, KV106, KV320, KVD40 and IGKC). In contrast, several regulators of the immune responses preferentially adsorbed to CaMg surfaces. This was the case for alpha-1-acid glycoproteins A1AG1 and A1AG2 (involved in inhibiting the immune cells and regulating the induction of IL-1 and IL-1β [41]). The haptoglobin (HPT), haptoglobin-related protein (HPTR) and albumin (ALBU) also showed increased adsorption on these surfaces. The HPT and HPTR are associated with the regulation of acute inflammation and tissue repair [42], and albumin is a well-known negative acute-phase regulator [43].

When comparing Ca and CaMg materials, we found that an immunoglobulin (HV551), a complement protein (CO8B) and two proteins associated with the regulation of immune responses (BLMH and CRP) were differentially adsorbed. Significantly reduced amounts of CRP and BLMH were found on Ca1.5Mg surfaces. The CRP is a positive acute-phase protein produced in response to inflammatory conditions [43,44], such as infection or trauma (in a Ca-dose-

dependent manner). The BLMH protein, known for regulating inflammatory chemokines (CXCL8 and GROα) and wound healing [45], also showed a lower affinity to Ca1Mg than Ca-doped material. *In vitro* inflammatory response to Ca depends on the ion concentration in a material [20], while Mg generally shows an anti-inflammatory activity [10]. Here, the CaMg sol-gel coatings displayed increased TNF-α and TGF-β secretion and gene expression. However, these coatings decreased IL-10 expression in the Mg-dose-dependent manner. Wang *et al*. [46] have developed an Mg-Ca phosphate cement that caused an increase in *TGF-β* gene expression and a reduction in the expression of *IL-6*, *IL-1β* and *IL-10*. These results indicate that such materials might affect the balance between pro- and anti-inflammatory proteins adsorbed onto the surface and cytokine release and gene expression of the cells. The final effect might depend on the relative amounts of Ca and Mg incorporated into the materials.

Another key process in bone regeneration is coagulation. The CaMg coatings preferentially adsorbed seven proteins associated with coagulatory processes (HRG, HBA, ZPI, FBLN1, HABP2, HEP2 and A2MG). Some other proteins (*e.g.,* FA11, FA10, FA9 and FA12) showed lowered affinity to these materials, depending on the concentration of Mg incorporated into the network. Thus, the comparison between Ca and CaMg coatings allowed us to understand better the effect of doping mixtures on protein adsorption. The addition of Mg led to an increase in the adsorption of 4 proteins (HRG, SPB12, PLMN and HBA) in a dose-dependent manner. The histidine-rich glycoprotein (HRG) exerts its anticoagulant effect by binding and neutralising heparin. As a result, it prevents the formation of heparin-antithrombin III complexes that inhibit activated coagulation factors (*e.g.,* thrombin) [40]. The plasminogen protein, PLMN, is the zymogen of plasmin, which dissolves the preformed fibrin clots and regulates wound healing, tissue remodelling, tumour metastasis and angiogenesis [47]. The Mg addition altered the protein adsorption patterns associated with this process and the coagulatory properties conferred by Ca might be changed in the CaMg materials.

For optimal tissue regeneration around a biomaterial, good cell adhesion is essential. The Mg ion is well known for promoting cell adhesion [48]. Therefore, it was not surprising that CaMg materials had increased affinity to proteins associated with cell adhesion processes (ZA2G, LG3BP, DSG1, FBLN1, DESP and HABP2). The observed changes in the surface area of MC3T3-E1 cells cultured on these materials support these results (except for Ca1.5Mg). It has been reported that increasing the amounts of Mg-phosphate mixed into Ca-phosphate cement from 0% to 10% causes cell spreading. However, Mg concentrations higher than 10% have the opposite effect [14]. These results suggest that incorporating more than certain amounts of Mg in a Ca-doped material does not enhance cell adhesion and spreading. Furthermore, the CaMg

materials showed a significantly lower affinity to proteins associated with this process (COMP, PCOC1, VTNC and IBP4).

Interestingly, the observed changes in ALP activity and osteogenic gene expression (*ALP*, *SP7*, *TGF-β* and *RUNX2*) depended on the concentration of Mg added to the coating. However, the effect was more evident for materials with a lower concentration of Mg. Similarly, Mg-Ca phosphate cements have been shown to promote osteogenesis both *in vitro* and *in vivo*, especially for materials with low Mg content [46]. In similarity to what has been observed for inflammatory responses, the amount of Mg added to Ca material could affect the cell response, either in an antagonistic or synergetic manner.

5. Conclusion

The main goal of this study was to understand how the mixtures of Ca and Mg incorporated into materials for bone regeneration affect *in vitro* cell responses and protein adsorption patterns. To achieve that, we developed and characterised new sol-gel coatings capable of controlled release of the Ca and Mg ions. Both ions were successfully incorporated into the sol-gel network without affecting the final cross-linking or forming crystalline structures. A controlled release of the ions was examined. Raising the proportion of Mg added to the network increased the amount of liberated Mg and Ca and the extent of material degradation. The CaMg materials, in comparison with the undoped network, generally adsorbed more proteins related to the regulation of inflammatory responses (A1AG1, A1AG2, HPTR, HPT and ALBU) and had reduced affinity to proteins associated with induction of inflammation (*e.g.*, immunoglobulins). Moreover, adding Mg and Ca together led to a decrease in the adsorption of significant inflammatory proteins (CRP and BLMH) with respect to Ca, showing the potential of Mg for controlling Ca-induced inflammation. *In vitro* responses of RAW264.7 macrophages showed that using the CaMg coatings led to an increase in TNF-α and TGF-β and a decrease in *IL-10* expression. Moreover, these coatings generally showed elevated adsorption of proteins related to cell adhesion (ZA2G, LG3BP, DSG1, FBLN1 and DESP). The increase in the MC3T3-E1 cell surface area depended on the amount of Mg incorporated into the material. Additionally, the *in vitro* assays showed that the ratio of Ca to Mg affected the ALP activity and osteogenic gene expression (*ALP*, *SP7* and *TGF-β*). With this, we can conclude that the desired equilibrium effect in ion mixtures depends on the amount of each ion added to the mix, rather than a simple sum of properties.

Conflicts of interest

There are no conflicts to declare.

Acknowledgements

The work was supported by Ministerio Ciencia e Innovación [PID2020-113092RB-C21; RTC-2017-6147-1], Generalitat Valenciana [GRISOLIAP/2018/091, APOSTD/2020/036, PROMETEO/2020/069], Universitat Jaume I [GACUJI/2021/14] and Basque Government [PRE_2017_2_0044]. The authors would like to thank Raquel Oliver, José Ortega, José Miguel Pedra and Iraide Escobés for their valuable technical assistance, and Antonio Coso (GMI-Ilerimplant) for making the titanium discs.

References

1 J. Jeong, J. H. Kim, J. H. Shim, N. S. Hwang and C. Yeong Heo, *Biomater. Res.*, 2019, **23**, 1–11.

2 M. Ansari, *Prog. Biomater.*, 2019, **8**, 223–237.

3 C. Dai, H. Guo, J. Lu, J. Shi, J. Wei and C. Liu, *Biomaterials*, 2011, **32**, 8506–8517.

4 E. O'Neill, G. Awale, L. Daneshmandi, O. Umerah and K. W. H. Lo, *Drug Discov. Today*, 2018, **23**, 879–890.

5 Y. Yan, Y. Wei, R. Yang, L. Xia, C. Zhao, B. Gao, X. Zhang, J. Fu, Q. Wang and N. Xu, *Colloids Surfaces B Biointerfaces*, 2019, **179**, 309–316.

6 N. J. Lakhkar, I. H. Lee, H. W. Kim, V. Salih, I. B. Wall and J. C. Knowles, *Adv. Drug Deliv. Rev.*, 2013, **65**, 405–420.

7 X. Yuan, H. Cao, J. Wang, K. Tang, B. Li, Y. Zhao, M. Cheng, H. Qin, X. Liu and X. Zhang, *Front. Immunol.*, 2017, **8**, 1196.

8 D. Liu, D. C. Genetos, Y. Shao, D. J. Geist, J. Li, H. Z. Ke, C. H. Turner and R. L. Duncan, *Bone*, 2008, **42**, 644–652.

9 E. Anitua, R. Prado, G. Orive and R. Tejero, *J. Biomed. Mater. Res. - Part A*, 2015, **103**, 969–980.

10 A. Cerqueira, F. Romero-Gavilán, I. García-Arnáez, C. Martinez-Ramos, S. Ozturan, R. Izquierdo, M. Azkargorta, F. Elortza, M. Gurruchaga, J. Suay and I. Goñi, *Mater. Sci. Eng. C*, 2021, **125**, 112114.

11 A. Cerqueira, I. García-Arnáez, F. Romero-gavilán, M. Azkargorta, F. Elortza, J. J. Martín de Llanos, C. Carda, M. Gurruchaga, I. Goñi and J. Suay, *Biomater. Adv.*, 2022, 212826.

12 B. Li, H. Cao, Y. Zhao, M. Cheng, H. Qin, T. Cheng, Y. Hu, X. Zhang and X. Liu, *Sci. Rep.*, 2017, **7**, 42707.

13 J. Sugimoto, A. M. Romani, A. M. Valentin-Torres, A. A. Luciano, C. M. Ramirez Kitchen, N. Funderburg, S. Mesiano and H. B. Bernstein, *J. Immunol.*, 2012, **188**, 6338–6346.

14 J. Zhang, X. Ma, D. Lin, H. Shi, Y. Yuan, W. Tang, H. Zhou, H. Guo, J. Qian and C. Liu, *Biomaterials*, 2015, **53**, 251–264.

15 Z. Othman, B. Cillero Pastor, S. van Rijt and P. Habibovic, *Biomaterials*, 2018, **167**,

191–204.

16 M. D. Swartzlander, C. A. Barnes, A. K. Blakney, J. L. Kaar, T. R. Kyriakides and S. J. Bryant, *Biomaterials*, 2015, **41**, 26–36.

17 F. Romero-Gavilán, A. M. Sanchez-Pérez, N. Araújo-Gomes, M. Azkargorta, I. Iloro, F. Elortza, M. Gurruchaga, I. Goñi and J. Suay, *Biofouling*, , DOI:10.1080/08927014.2017.1356289.

18 F. Romero-Gavilán, A. Cerqueira, E. Anitua, R. Tejero, I. García-Arnáez, C. Martinez-Ramos, S. Ozturan, R. Izquierdo, M. Azkargorta, F. Elortza, M. Gurruchaga, I. Goñi and J. Suay, *J. Biol. Inorg. Chem.*, 2021, **26**, 715–726.

19 M. Martinez-Ibañez, M. J. Juan-Diaz, I. Lara-Saez, A. Coso, J. Franco, M. Gurruchaga, J. Suay Anton and I. Goñi, *J. Mater. Sci. Mater. Med.*, , DOI:10.1007/s10856-016-5690-9.

20 F. Romero-Gavilán, N. Araújo-Gomes, A. Cerqueira, I. García-Arnáez, C. Martínez-Ramos, M. Azkargorta, I. Iloro, F. Elortza, M. Gurruchaga, J. Suay and I. Goñi, *J. Biol. Inorg. Chem.*, 2019, **24**, 563–574.

21 F. Romero-Gavilán, N. C. Gomes, J. Ródenas, A. Sánchez, F. , Mikel Azkargorta, Ibon Iloro, I. G. A. Elortza, M. Gurruchaga, I. Goñi and and J. Suay, *Biofouling*, 2017, **33**, 98–111.

22 N. Araújo-Gomes, F. Romero-Gavilán, I. García-Arnáez, C. Martínez-Ramos, A. M. Sánchez-Pérez, M. Azkargorta, F. Elortza, J. J. M. de Llano, M. Gurruchaga, I. Goñi, J. Suay, J. J. Martín de Llano, M. Gurruchaga, I. Goñi and J. Suay, *JBIC J. Biol. Inorg. Chem.*, 2018, **23**, 459–470.

23 A. Cerqueira, F. Romero-Gavilán, N. Araújo-Gomes, I. García-Arnáez, C. Martinez-Ramos, S. Ozturan, M. Azkargorta, F. Elortza, M. Gurruchaga, J. Suay and I. Goñi, *Mater. Sci. Eng. C*, 2020, **116**, 111262.

24 F. Romero-Gavilan, N. Araújo-Gomes, A. M. Sánchez-Pérez, I. García-Arnáez, F. Elortza, M. Azkargorta, J. J. M. de Llano, C. Carda, M. Gurruchaga, J. Suay and I. Goñi, *Colloids Surfaces B Biointerfaces*, 2018, **162**, 316–325.

25 F. Romero-Gavilán, S. Barros-Silva, J. García-Cañadas, B. Palla, R. Izquierdo, M. Gurruchaga, I. Goñi and J. Suay, *J. Non. Cryst. Solids*, 2016, **453**, 66–73.

26 F. Romero-Gavilán, J. Carlos-Almeida, A. Cerqueira, M. Gurruchaga, I. Goñi, I. M. Miranda-Salvado, M. H. Vaz Fernandes and J. Suay, *Prog. Org. Coatings*, , DOI:10.1016/j.porgcoat.2020.105770.

27 G. Chernev, N. Rangelova, P. Djambazki, S. Nenkova, I. Salvado, M. Fernandes, A. Wu and L. Kabaivanova, *J. Sol-Gel Sci. Technol.*, 2011, **58**, 619–624.

28 F. Romero-Gavilán, N. Araújo-Gomes, I. García-Arnáez, C. Martínez-Ramos, F. Elortza, M. Azkargorta, I. Iloro, M. Gurruchaga, J. Suay and I. Goñi, *Colloids Surfaces B Biointerfaces*, 2019, **174**, 9–16.

29 A. Jemat, M. J. Ghazali, M. Razali and Y. Otsuka, *Biomed Res. Int.*, , DOI:10.1155/2015/791725.

30 S. Yoshizawa, A. Brown, A. Barchowsky and C. Sfeir, *Acta Biomater.*, 2014, **10**, 2834–2842.

31 P. Saravanapavan, J. Selvakumaran and L. L. Hench, in *Key Engineering Materials*, Trans Tech Publications Ltd, 2004, vol. 254–256, pp. 785–788.

32 M. C. Carroll, *Nat. Immunol.*, 2004, 5, 981–986.

33 C. Skerka, Q. Chen, V. Fremeaux-Bacchi and L. T. Roumenina, *Mol. Immunol.*, 2013, **56**, 170–180.

34 J. J. Alexander, J. S. Sankaran, K. L. Seldeen, R. Thiyagarajan, A. Jacob, R. J. Quigg, B. R. Troen and S. Judex, *Immunobiology*, 2018, **223**, 761–771.

35 R. Bouillon, F. Schuit, L. Antonio and F. Rastinejad, *Front. Endocrinol. (Lausanne).*, 2020, **10**, 910.

36 P. White and N. Cooke, *Trends Endocrinol. Metab.*, 2000, **11**, 320–327.

37 G. Falgarone and G. Chiocchia, *Adv. Cancer Res.*, 2009, 104, 139–170.

38 N. H. Cho and S. Y. Seong, *Immunology*, 2009, **128**, 479–486.

39 D. C. Kilpatrick and J. D. Chalmers, *J. Biomed. Biotechnol.*, , DOI:10.1155/2012/138797.

40 I. K. H. Poon, K. K. Patel, D. S. Davis, C. R. Parish and M. D. Hulett, *Blood*, 2011, **117**, 2093–2101.

41 M. Bteich, *Heliyon*, 2019, **5**, e02879.

42 D. J. Schaer, F. Vinchi, G. Ingoglia, E. Tolosano and P. W. Buehler, *Front. Physiol.*, 2014, **5**, 415.

43 S. Jain, V. Gautam and S. Naseem, *J. Pharm. Bioallied Sci.*, 2011, **3**, 118–127.

44 N. R. Sproston and J. J. Ashworth, *Front. Immunol.*, 2018, **9**, 754.

45 R. Riise, L. Odqvist, J. Mattsson, S. Monkley, S. M. Abdillahi, C. Tyrchan, D. Muthas and L. F. Yrlid, *Sci. Rep.*, 2019, **9**, 1–10.

46 M. Wang, Y. Yu, K. Dai, Z. Ma, Y. Liu, J. Wang and C. Liu, *Biomater. Sci.*, 2016, **4**, 1574–1583.

47 D. Barthel, S. Schindler and P. F. Zipfel, *J. Biol. Chem.*, 2012, **287**, 18831–18842.

48 H. Zreiqat, C. R. Howlett, a. Zannettino, P. Evans, G. Schulze-Tanzil, C. Knabe and M. Shakibaei, *J. Biomed. Mater. Res.*, 2002, **62**, 175–184.